CFD analysis of a Darrieus Vertical-Axis Wind turbine installation on the rooftop of a buildings under turbulent inflow conditions

Pradip Zamre[1] and Thorsten Lutz[1]

[1]University of Stuttgart, Institute of Aerodynamics and Gas Dynamics, Pfaffenwaldring 21, D-70569 Stuttgart, Germany

Correspondence: Pradip Zamre (zamre@iag.uni-stuttgart.de)

Abstract.

The behavior of a rooftop mounted generic H-rotor Darrieus vertical axis wind turbine (H-VAWT) is investigated numerically in realistic urban terrain. The interaction of the atmospheric boundary layer with the different buildings, topography, and vegetation present in the urban environment leads to the highly turbulent inflow conditions with continuously changing inclination, and direction. Consequently, all these factors can influence the performance of a VAWT significantly. In order to simulate a small H-VAWT at rooftop locations in the urban terrain under turbulent inflow conditions, a computational approach is developed. First, the flow field in the terrain is initialized and computed with inflow turbulence. Later, the wind turbine grids are superimposed for further computation in the turbulent flow field. The behavior of the H-VAWT is complex due to the 3D unsteady aerodynamics resulting from continuously changing the angle of attack, blade wake interaction, and dynamic stall. To get more insights into the behavior of a rooftop mounted H-VAWT in turbulent flow, high fidelity DDES simulations are performed at different rooftop positions and compared the results against the behavior at uniform inflow conditions in the absence of inflow turbulence, built environment. It is found that the performance of wind turbine is significantly increased near the rooftop positions. The skewed flow at the rooftop location increases the complexity. However, this effect contributes positively to increasing the performance of wind turbines.

1 Introduction

Wind energy is available in abundance, but it is not uniformly distributed. The growth of wind energy is related to large-scale horizontal axis wind turbines (HAWTs), and wind farms located onshore and offshore. Though it is known for its potential, the good offshore sites and unexploited windy areas are decreasing. Considerable losses are associated with energy transportation from source to places where it is consumed. Distributed and decentralized wind power is associated with the application of small, medium and, lower end of large wind turbines (up to 2MW) in remote deployment or small-scale wind farms. Distributed and decentralized power generation emerges as complementary infrastructure to the conventional power system that envisions electricity generation close to the consumption site e.g. urban/suburban environment, lowering the capital investments in transmission lines. The concept of urban wind energy is not new. There have been already efforts to investigate the feasibility of harnessing the urban wind by installing small wind turbines on the roof of existing buildings or as stand-alone deployment in an urban area (Balduzzi et al., 2011; Mithraratne, 2009; van Wijk, 2011; Toja-Silva et al., 2013). The wind turbines can also

be integrated with buildings, designed aerodynamically to accelerate the wind (KC et al., 2019; Karadag and Yuksek, 2020). It is a well-known fact that the mean wind speed in urban environments is lower than in open areas or rural areas. However, some locations tend to be windier such as rooftops, building edges, a passage between two buildings, etc. The interaction of the atmospheric boundary layer with the rough terrain and obstacle of different shapes and permeability present along the flow path

30 leads to complex flow conditions in the built environment with lower velocities, high turbulence, and continuously changing direction. These conditions can severely influence the behavior and dynamic loads of the small wind turbine.

1.1 VAWT in turbulent urban flow field

In general, the research areas of urban wind energy and small wind turbines overlap ~~with~~ each other. In the wind industry, wind turbines can be classified ~~based on their axis of rotation~~ in two categories, namely horizontal and vertical axis wind

35 turbines. The horizontal axis wind turbine concept has been proven mature, successful, and economical on a large scale, but it is wind direction-dependent. ~~Furthermore,~~ it needs a yaw mechanism. In the built environment, the flow inclinations negatively affect the performance of a small HAWT (Bianchi et al., 2013). In this regard, the VAWT concept has several advantages in the urban environment. In skewed flow, the performance of the H-Darrieus VAWT rotor increases above the non-skewed flow (Mertens et al., 2003). It has the omni-direction capability. Thus no yaw mechanism is needed, which reduces mechanical

40 complexity. VAWTs typically have fewer moving parts, and a generator can be installed at ground level. It could lead to lower maintenance costs and higher availability. The wake recovery of VAWT is faster than in case of the HAWT which allows a dense cluster of wind turbines in the wind farm, increasing the power density. Also, the VAWT concept has potentially lower noise emissions than the HAWT of the same power class (Kern et al., 2019). However, the VAWT concept has some drawbacks. Its performance is lower than that of HAWT. The underlying physics behind the operating of VAWT is more complex than

45 HAWTs. The inherent unsteadiness is caused by the continuously changing angle of attack and relative velocity during the revolution.

The influence of turbulence on the behavior of the VAWT is one of the significant research areas considering the applications of small VAWT in urban environments. One approach to investigating the influence of the turbulence effects on the VAWT is based upon correlating the performance and on-site wind measurements. Möllerström et al. (2016) studied a 200 kW Darrieus

50 VAWT in the open field. They concluded that turbulence positively impacts energy extraction, and the effect is more evident at higher tip-speed ratios. Also, the performance of the wind turbine and optimal lambda increase with TI allowing optimization of control strategies to capture more high-energy wind gusts. Bertényi et al. (2012) also found that turbulence has no adverse effect on the performance of VAWT using "gust tracking". Pangini et al. (2015) compared the performance of a small commercial VAWT with HAWT of the same rated capacity of 20 kW installed at the Savona harbor. It is concluded that both wind turbines

55 are sensitive to turbulence and not suitable for installation in complex areas where turbulence levels are often high. Kooiman and Tullis (2010) studied the effects of wind velocity and direction fluctuations on the energy production of rooftop installed VAWTs in urban environments. The output power varied with wind velocity fluctuations but was roughly independent of the wind direction changes. They also compared data from urban environment testing with the earlier work of Bravo et al. (2006) on the same wind turbine in a low turbulence wind tunnel. It is found that the performance of wind turbine degraded marginally

60   at TI < 15% compared to the smooth flow benchmark at TI < 2%. There is not consistency in the findings of discussed studies about the influence of the turbulence on the the behavior of VAWT. Also, replicating the flow characteristics from the urban environment in the wind tunnel poses serious challenges. Most of the wind tunnel facilities are designed for aerospace research with very low background turbulence intensity. ~~One may argue that the~~ turbulence intensity in an urban environment can easily exceed 10%. The eddies size differs over a broader range of integral length scales. These factors limit the scope of addressing

65   the topic of turbulence in the wind tunnel.

   The advancement in computing capacities and infrastructure allows the use of high-fidelity computational fluid dynamics (CFD) methods ~~extensively~~ to investigate complex flow behavior. A broader range of approaches has been used to explore different aerodynamics phenomena of the VAWT. One of the earliest studies to model the influence of inflow turbulence on the VAWT was carried out by Brahimi and Paraschivoiu (1995). The effect of turbulence intensity on the performance of an

70   offshore VAWT was investigated by Siddiqui et al. (2015) and found that performance deteriorates by almost 23% to 42% as turbulence intensity increases from 5% to 25%. Rezaeiha et al. (2018) studied the impact of different operational parameters on an H-Darrieus rotor along with turbulence intensity. He found that the dynamic stall at a low tip speed ratio is delayed with an increase in turbulence level and the performance coefficient increases. However, at the optimal tip speed ratio, the turbulence has a relatively marginal influence. Also, the turbulence reduces the impact of the shaft wake on the blade forces in downwind

75   passage. All these studies primarily focused on the influence of turbulence on the performance of the VAWT in controlled conditions and not in realistic conditions ordinarily present in the urban environment. Siddiqui et al. (2021) analyzed the effect of turbulence and ground clearance on the performance of a rooftop VAWT using three-dimensional RANS simulations. Contrary to Mertens et al. (2003), it was found that the performance of a VAWT enhanced at height, offering less ground shearing effect. Also, with increasing turbulence intensity, a drop in performance is observed. To the author's knowledge, there

80   are no high fidelity DDES or LES studies of a rooftop mounted H-Darrieus rotor available in realistic urban terrain under turbulent inflow conditions.

1.2   Scope and objectives

This work aims to investigate the aerodynamic performance of a rooftop mounted H-Darrieus rotor vertical axis wind turbine in a realistic urban environment under turbulent inflow conditions considering the topography, different buildings, and large

85   vegetation area. A large area is considered for the investigation to mimic the development of a realistic urban boundary layer. A generic reference H-Darrieus rotor is scaled up based on the geometrical parameter for the present work. As a basis for comparison, the scaled-up variant is analyzed at the uniform flow conditions. With the existing high-fidelity process chain, the characteristic of an H-Darrieus rotor at different heights over the rooftop of different buildings can be analyzed under resolved turbulent conditions. Variations in height are aimed at investigating the wind turbine performance in different turbulence levels

90   and inclinations. The coefficient of power, normal and tangential loads are compared with the reference case at the uniform inflow.
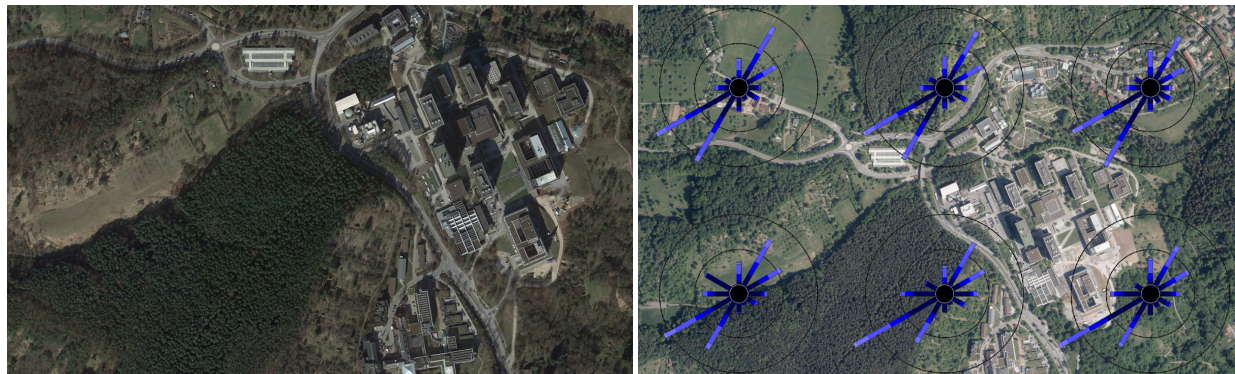
Figure 1. Aerial view Morgenstelle campus (© Google Earth 2020), Wind-rose from synthetic wind statistics (© 2021 Landesanstalt für Umwelt Baden-Württemberg)
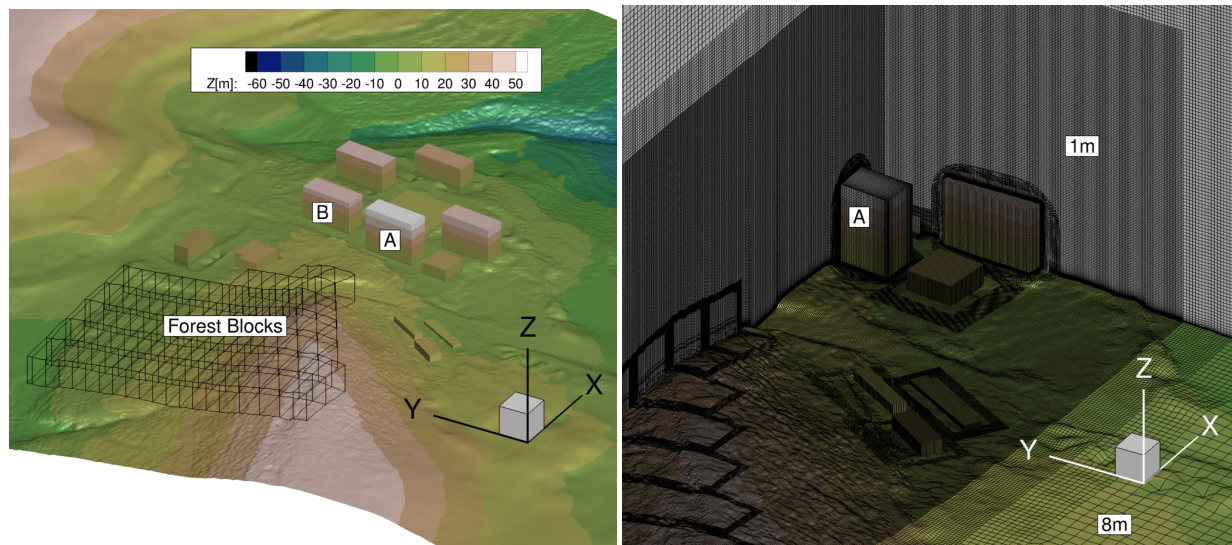
Figure 2. The urban terrain model and computational grid)

2 Numerical Process chain

2.1 CFD solver

The FLOWer is a compressible, block-structured Reynolds Averaged Navier Stokes (RANS) solver developed by the German
Aerospace Center (DLR) (Rossow et al., 2014) and is continuously furthered to incorporate new features and improve the
performance at the Institute of Aerodynamics and Gas Dynamics (IAG, University of Stuttgart). The overlapping grid technique
CHIMERA enables the assembly of independent grids of each component by embedding them into a background mesh (Benek

et al., 2014). Furthermore, the solver is extended with the functionality of higher-order finite difference weighted essentially non-oscillatory (WENO) scheme (Schäferlein et al., 2014), and different Detached Eddy Simulation (DES) models (Weihing et al., 2018). Also, it has been extended with vegetation modeling capabilities (Letzgus et al., 2018). The FLOWer has proven capabilities for wind turbine and helicopter simulations in several projects.

2.2 Generation of inflow turbulence

The inflow turbulence is generated using the in-house code PROFGEN, which is adopted from the work of Mann (1992). This model is based on the von Karman iso-tropic spectrum $\phi(\kappa)$ and uses the rapid distortion theory to estimate the effect of shear. Three input parameters are required: length scale l_0, stretching factor Γ, and energy dissipation $\alpha\epsilon^{2/3}$. Moreover, l_0 and $\alpha\epsilon^{2/3}$ determine the magnitude and the distribution of energy in the spectral domain. Γ controls the level of shear and anisotropy.

The fluctuating components of atmospheric turbulence u' are transformed into a volume force term $\boldsymbol{f}_s$ and is applied to a transverse plane downstream from the inlet. It is defined as force per unit volume applied to accelerate the mean velocity field from $\bar{\boldsymbol{u}}$ to $\bar{\boldsymbol{u}} + \boldsymbol{u}'$, and as per Troldborg et al. (2014), is given by

$$\boldsymbol{f}_s = \frac{\rho \boldsymbol{u}'}{\Delta x}(\bar{u}_n + \frac{1}{2}u'_n) \tag{1}$$

Here $\bar{u}_n$ and u'_n, are the magnitude of the mean and the fluctuating velocity with index n and Δx is the grid spacing normal to the transverse plane.

2.3 Vegetation modeling

The forest blocks are modeled as a porous medium. The drag caused by the vegetation is added to the momentum and energy equations of the Navier-Stokes equations via the volume force source term. It is based on the approach of Shaw et al. (1992). The drag depends on the local foliage density $a(z)$. It is possible to model the forest heterogeneously, considering local foliage density and height values for different parts of the vegetated area. The drag source term is given by

$$F_w = -\rho c_d a(z)|u|\boldsymbol{u} \tag{2}$$

where, ρ, c_d, $|u|$ and $\boldsymbol{u}$ are density, the drag coefficient, local magnitude of velocity, and velocity vector. The Leaf Area Index (LAI) over the height is defined as

$$LAI = \int\limits_z^h a(z)dz \tag{3}$$

A lower value of LAI represents sparse vegetation, while higher values of LAI represents dense vegetation.

2.4 Computational set-up

2.4.1 The H-Darrieus Turbine and its scaling

125 The examined wind turbine is based on a generic two-bladed H-rotor VAWT designed by Li et al. (2016) with the airfoil section NACA0021. Also, it has been investigated experimentally in the wind tunnel as well as in the field. It has a diameter of 2 m, a blade height of 1.2 m, and a blade chord length of 0.265 m. The blade cross-section area is constant over the complete length. The central shaft has a diameter of 0.216 m. For rooftop application in present work, it is scaled up by a factor of 3.5, keeping the geometrical parameter solidity constant. The solidity σ is calculated as follows

130
$$\sigma = \frac{nc}{D} \tag{4}$$

where n is the number of blades, c is the blade chord length, and D is the diameter of a VAWT.

Table 1. Scaling-up of VAWT

Parameter	Original	Scaling Factor 3.5
Wind speed ($\mathrm{ms^{-1}}$)	8	8
Rotor diameter D (m)	2	7
Blade length L (m)	1.2	4.2
Blade chord c (m)	0.265	0.9275
Aspect ratio (L/D)	0.6	0.6
Turbine solidity (nc/D)	0.265	0.265

The scaled version has a rotor diameter of 7 m, a blade height of 4.2 m, a blade chord length of 0.9275 m, and a central shaft diameter of 0.756 m. It has a fixed pitch of 6° which remains constant over the revolution. The dimensions for the original and the scaled-up version are shown in table 1. ~~The aspect ratio does not change after scaling~~.

135 #### 2.4.2 Terrain and wind direction

For the investigation, the "Morgenstelle" campus of the University of Tübingen from south Germany is selected as depicted in Fig. 1. ~~Also, the~~ synthetic wind atlas data presented in Fig. 1 shows the southwest as the main wind direction with densely forested hill lying in the upstream region of the built environment. There are 4-5 high-rise buildings with a height of 40 m and more.
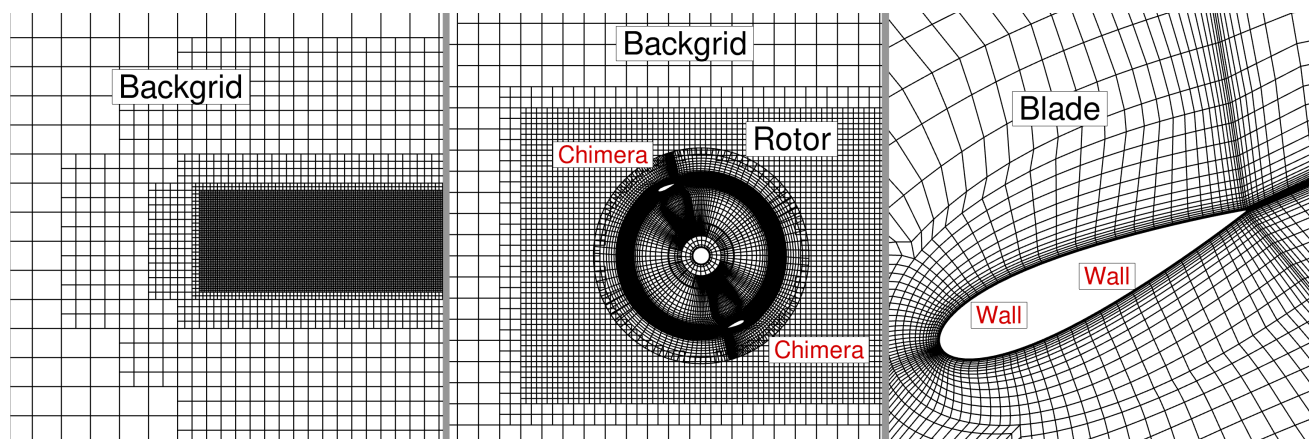
Figure 3. Computational grid of the H-VAWT for the uniform inflow study. Boundary conditions are shown in red colored text. (Not to the scale and every fourth cell of the mesh has been shown.)

2.4.3 CFD model

The wind turbine at the original scale is numerically investigated and validated using the FLOWer flow solver at IAG by Dessoky et al. (2019). As described in section 2.4.1, the grids are also scaled with same the scaling factor as a wind turbine. The blades and shaft grids have a fully resolved boundary layer ($y^+ \leqslant 1$) with 32 cell layers. The shaft is considered only in the region of the rotor. The blades are meshed using Pointwise and Gridgen commercial mesh generation applications. Based on the convergence study for different grids with the original wind turbine with FLOWer, the blade mesh is composed of 336 cells in the chord-wise direction and 48 cells in the span-wise direction. The CHIMERA intersection area is defined near the outer periphery of the rotating zone to assemble the wind turbine in the background grid. There are no changes made in the wind turbine grid throughout the study.

The computational approach is discussed in the next section 2.5. For the investigations in uniform inflow, the background grid is created by using the in-house automated tool. The background grid is a Cartesian type of dimension 215 m x 84.5 m x 76.8 m in x,y, and z-direction, respectively. The grid has hanging nodes enabling different levels of refinements. However, the background grid used for the uniform flow condition is not shown in this article. The near wake region has a grid refinement size of 8.625% of the chord shown in fig. 3. No inflow turbulence is applied. The background grid specific to the uniform inflow investigations is not relevant to the urban terrain investigations.

In the case of urban terrain simulations, the computation grids for the buildings are created using Pointwise and Gridgen. Different building structures, terrain, forested blocks, and the assembly of the computation grids are shown in fig. 2. The Cartesian background grid of the terrain has the smallest cell size of 1 m in the region of interest, transiting to 8 m resolution in the remaining domain by the usage of hanging nodes. In order to resolve the inflow turbulence, a channel-like region from inlet to outlet is meshed with a resolution of 1 m which covers all the considered built environment along with the forest and topographical features. It results in 105 Million cells in the background mesh. The boundary layer is resolved with (y^+
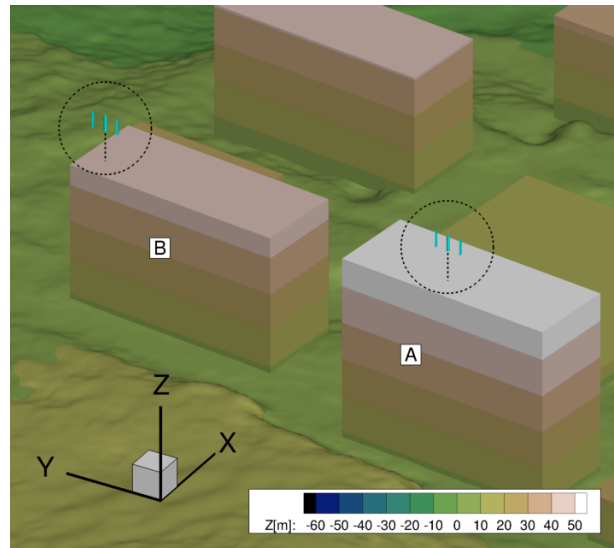
Figure 4. Rooftop mounted H-VAWTs ~~over~~ A and B

$\leqslant 2$) with 64 layers for the terrain and buildings. The extent of the background mesh is 1087 m × 2432 m × 655 m in x,y, and z-direction, respectively. The chosen values of LAIs for forest blocks vary from 1.8 to 2.0, corresponding to the winter season. For the investigation of the wind turbines in urban terrain, ~~overall,~~ a complete set-up consists of background mesh, two rotors, shafts, wake refinement region and remaining built structures along with vegetation. Figure 4 shows the rooftop

165 mounted H-VAWTs ~~over~~ A and B. It has approximately 169 million cells and 21000 blocks.

2.4.4 Boundary conditions and solver setup

In the case of ~~investigation in~~ uniform inflow with wind velocity 8 ms^{-1}, Farfield boundary conditions are defined for all the sides of the computational domain. All the components of the turbine are treated as a No-slip wall.

For the investigation in the urban terrain, a generic log law profile based on ~~data from~~ the New European Wind Atlas

170 is defined via a Dirichlet boundary condition at the inlet. At the start of the simulation, the whole computational domain is initialized with this wind profile. The lateral sides, topside, and outlet are realized as Farfield boundary conditions with zero-order extrapolation. The ground and the surfaces of the rotors and the built environment are defined as a No-slip wall. The input parameters, turbulence intensity of 10%, and a length scale of 50 m are used to generate inflow turbulence as per Kaimal spectrum for PROFGEN. ~~It was~~ introduced using body forces on the transverse plane at 96.5 m downstream from the inlet and

175 approximately 450 m upstream from the built environment under consideration.

For the present work, DDES simulations ~~were~~ performed employing a dual time-stepping scheme for temporal discretization. Menter-SST model is used for turbulence modeling (Menter, 1994). A second-order scheme with the Jameson-Schmidt-Turkel (JST) artificial dissipation term (Jameson, 1981) is used for spatial discretization in the boundary layer. The fifth-order WENO
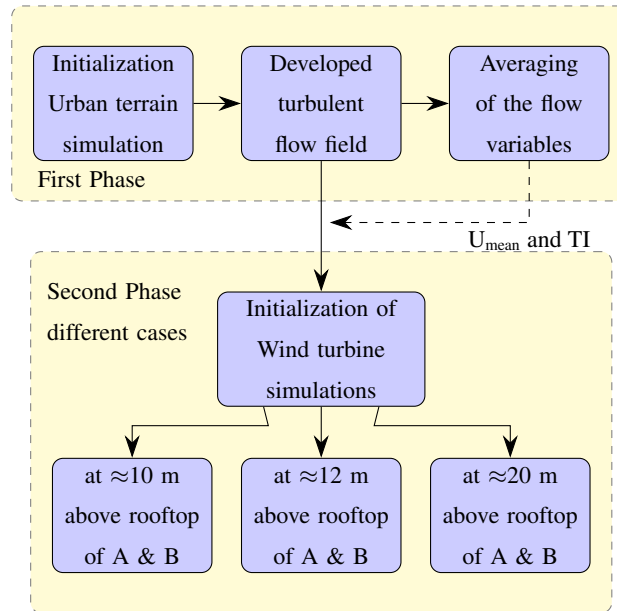
Figure 5. Computational approach for the investigation of VAWT in urban terrain under turbulent inflow conditions

scheme is applied to the background mesh to ensure less numerical dissipation and reconstruction of fluxes and more accurate
180 propagation of vortical, turbulent structures.

2.5 Computational approach

In the absence of the experimental or field measurements for the scaled-up VAWT, the performance at uniform flow conditions without inflow turbulence is considered a basis for comparison with realistic conditions. Ferreira et al. (2007) studied 2D VAWT numerically and experimentally. They showed that the delayed eddy simulations (DES) results reasonably predict the
185 generation and shedding of vorticity and exhibit acceptable sensitivity to spatial and temporal grid refinement. It implies that scale resolving DES simulations can be used where validation data is limited or nonexistent. Therefore in the present work, the scaled-up VAWT is investigated first by applying a high-fidelity approach at the reference condition of uniform inflow 8 ms^{-1} for different operating points. The power coefficient vs. tip speed ratio ($Cp - \lambda$) curve serves as one of the basis for selecting the operating point and comparing the behavior of the wind turbine in realistic urban terrain.
190   In order to have a well-developed flow field before the investigation of the wind turbines in urban terrain, the simulations are divided into two distinct phases, as depicted in fig. 5. In the first phase, the urban landscape is simulated without wind turbines with turbulent inflow. Once the flow field is well developed in the domain, averaging of the flow variables is started. This point also serves as the start for the wind turbine simulations. The mean wind profile, turbulence intensity, and skew angles are derived from the averaged solution.
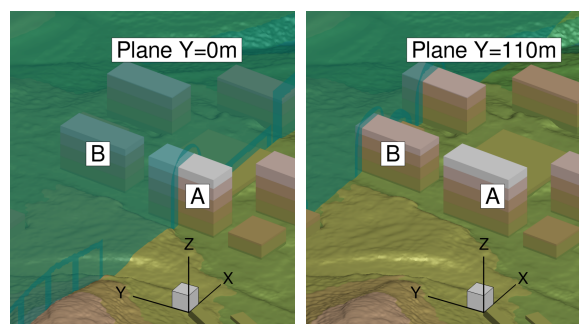
Figure 6. Post-processing planes passing through A and B

As per recommended practices for the deployment of the wind turbines in the built environment (Fields et al., 2016), for the rotors more than 2 m diameter, the heights for the reaching the acceptable wind speed and turbulence intensity should be the bottom of the rotor swept area. Siddiqui et al. (2021) investigated the effect of ground clearance on the performance of a rooftop mounted VAWT and observed optimal performance of the wind turbine at height 7.5 and 10 times of the chord above the rooftop. Here, the height is measured from the lower blade tip to the rooftop. Therefore, based on the local averaged wind speeds and turbulence intensity, three different heights 10 m, 12 m and 20 m are selected to investigate the behavior of the H-VAWT in the present work. In the resulting configurations, the lower blade tips are at approx. 8.5, 10.7, and 19.3 times of chord length from the rooftop, respectively. The rationale behind selecting the 20 m height is that to compare the performance of the H-VAWT near rooftop positions to the relatively away position, which is less influenced by the geometry of the buildings.

In the second phase, the wind turbine and wake refinement region are introduced to the urban terrain's existing computational set-up and flow field and computed further. The flow field in the refinement region is interpolated from the background grid's existing solution, and the wind turbine structures are initialized with reference flow velocity and calculated further. This approach helps to save some computational costs. If the wind turbines are simulated in urban terrain from the start, it will increase the computation cost drastically as the pace of the simulation is limited by the small-time steps required for the wind turbines. In this approach, as the wind turbines are not present in the first phase, the domain can be simulated with a relatively larger time step than the wind turbine simulations. It is assumed that the wind turbine is rotating at constant rotational speed under turbulent inflow. The rotational speeds are determined from the averaged local wind velocity over a longer period and the selected tip-speed ratio as an operating point. The active pitch control or dynamic changes in rotation speed as per variations in the incoming wind are not considered.

To sum up, there are three different cases with individual objectives are included in the present work. In the first case, investigations are carried out at uniform flow conditions. In the second case, the turbulent flow field in the urban terrain is analyzed, while in the third case, the wind turbines in urban terrain under turbulent conditions are investigated.

2.6 Evaluation

The scaled-up variant of the H-Darrieus rotor is evaluated at reference conditions. After some revolutions, the forces and moment converge, and the trend shows periodic nature. Revolutions after this point are considered for evaluation. The moment is averaged to calculate the power coefficient for the C — λ curve at reference conditions.

In urban terrain simulations, the flow field is averaged after turbulence is propagated through the complete domain. It is needed to evaluate the flow conditions at the rooftop. The post-processing plane Y= 0 m passes through building A while Y= 110 m passes through building B. Based on the averaged velocity profiles and turbulence intensity, two different locations are identified at the rooftop of building A and B. At these locations, the wind turbine is placed at three distinct heights of 10 m, 12 m, and 20 m from the rooftop to investigate the influence of the skewed flow over the buildings.

At a later stage, the wind turbines are simulated for a total of 42 revolutions after initialization. The variables are considered after wind turbines complete 12 revolutions as some time is needed to develop the near wake. From previous experiences, approximately four revolutions are required at reference conditions to obtain convergence in the variables such as moment and forces and near wake flow field.

3 Results and discussion

The results are presented in three different subsections. The first subsection 3.1 investigates scaled H-VAWT at uniform conditions without any terrain and inflow turbulence. The second subsection 3.2 presents the flow field analysis of the urban terrain under inflow turbulence without wind turbines. Subsequently, the behavior of the rooftop mounted H-VAWTs in realistic conditions at different heights are discussed in subsection 3.3.

3.1 Wind turbine simulations at uniform inflow conditions

This section compares the power coefficient, blade forces, and moment of the scaled-up wind turbine at different tip-speed ratios under uniform inflow conditions with wind speed 8 ms^{-1}. After near wake development, periodic nature is observed for the variables over the revolutions. The tip-speed ratios are selected from the range low $\lambda = 1.2$ to high $\lambda = 4.0$. For the investigation, the rotational speed of the wind turbine was adjusted as per the tip speed ratio keeping the free-stream velocity constant.

Figure 7 shows the variations of a single blade's normalized moment, tangential and normal forces for the different tip speed ratios over the last revolution. Increasing λ results in the complex nature in moment and forces. In the absence of the inflow turbulence, the unsteady effects on the loads and moment come from the phenomena like continuous change in angle of attack, blade-vortex interaction, blade wake interaction involved in the operation of VAWT itself. The sinusoidal nature can be seen in the moment curves in the first half revolutions for all the operating points in the first plot. This part contributes the most to the moment generation. In the beginning of the revolution $(0° \leq \theta° \leq 30°)$, increasing λ results in lower moments. Except $\lambda =1.2$ for all other operating points at azimuth positions $75° \leq \theta° \leq 180°$, moment increases rapidly, reaches a maximum around

WIND
ENERGY
SCIENCE
DISCUSSIONS
european academy of wind energy
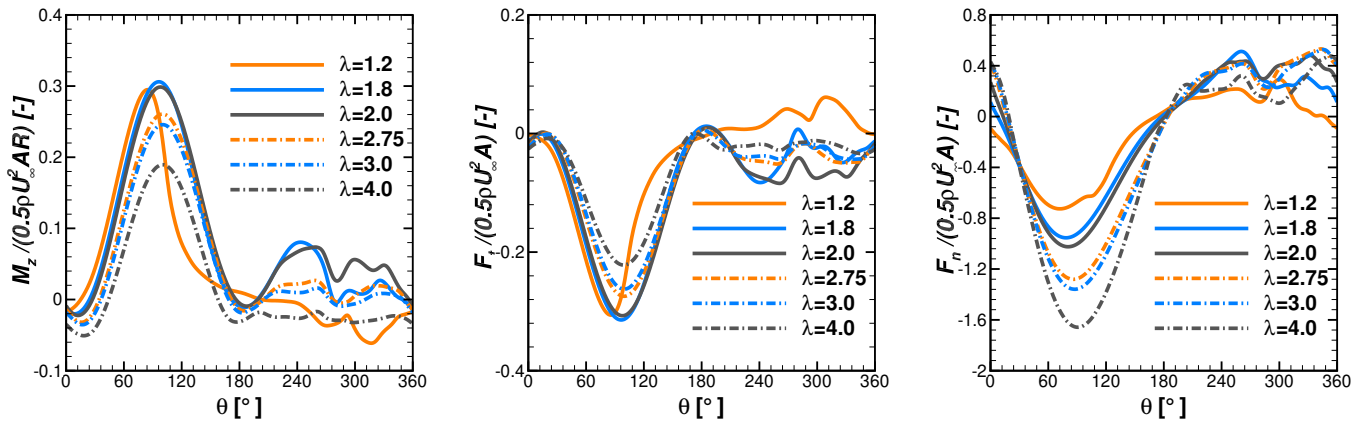
Figure 7. Normalised moment, tangential and normal forces of a single blade at different tip-speed ratio under reference conditions with uniform inflow $8~\mathrm{ms}^{-1}$ without terrain

90°-100°, and then decreases reaching to zero or negative at 180°. Due to the rotational frame of reference, the notations for the tangential force are opposite to the moment. Tangential force, which is responsible for the production of the moment,

250 shows correlation with the moment in second plot. Except λ =1.2, with increasing tip speed ratio, the normalized tangential force also increases between $75° \leq \theta° \leq 180°$. The negligible difference is observed in peak moment and tangential force for λ =1.8 and 2.0. In the case of λ =1.2, the rapid decrease in the moment and tangential force can be attributed to the dynamic stall phenomena, which is persistent at low tip speed ratio. This is in line with the behavior of the un-scaled H-VAWT, which has been studied by Bangga et al. (2017) for the dynamic stall phenomenon. Also, Rezaeiha et al. (2018) performed 2.5D

255 simulations for the a two-bladed H-VAWT with airfoil NACA0012 for the influence of the operational parameters. They found similar behavior at lower λ while studying the influence of the tip speed ratio on the performance.

In the second half revolutions ($180° \leq \theta° \leq 360°$), the moments and tangential forces show a not linear trend. The wind speed experienced by a blade for these azimuth positions is slowed down due to the moment extraction in the first half revolutions, which leads to the stalled conditions. Also, the blade wake interactions dominate in the second half revolutions.

260 Therefore, fluctuations can be seen in the moment and tangential forces. The influence of the wake arising from the shaft can be distinguished by the sudden drops and jumps around 270°. Compared to other operating points, λ =1.8 and 2.0 generate a relatively higher moment in the second half revolution. However, the magnitude is far lower than the first half of the revolution. With increasing λ, the nature of the curve flattens in the second half of the revolutions.

The third plot of fig. 7 shows variations in the normalized normal forces experienced by a single blade over revolution for

265 different tip-speed ratios. At 0°, the blade is almost aligned with the flow direction and experiencing a small angle of attack. As the blade moves further over azimuth, the normal force decreases, gradually reaching a minimum around azimuth 100-105° as the blade position is normal to the flow direction and then increases. In the considered notation, when directed towards the axis of rotation, the force has a "negative sign". When force is directed away from the axis of rotation, it has a "positive sign".
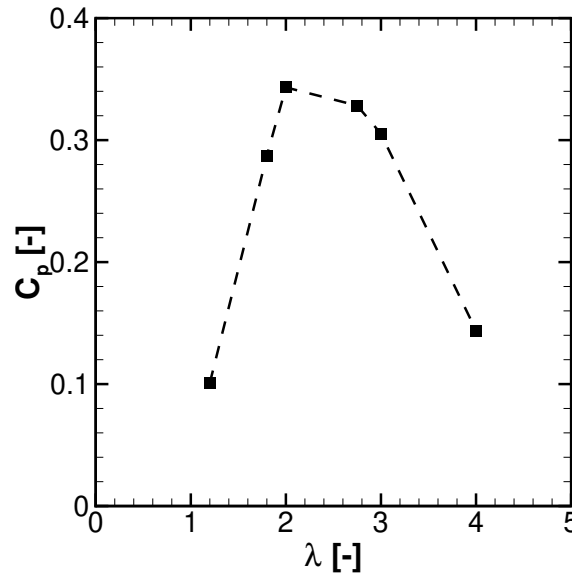
Figure 8. Power coefficient for different tip speed ratios (λ) at uniform inflow conditions 💬

After 180° azimuth position, the direction of the force is reverted. The influence of the wake coming from the shaft can be seen around 270°. Unlike the moment and tangential force, the normal force increases with the increasing tip-speed ratio over the considered range.

The ~~coefficients of~~ power for different operating points are shown in fig. 8. The C_p increases with λ. The maximum C_p occurs between $\lambda = 2$ and 2.75, and then it decreases. The power coefficient differs despite having a similar trend for $\lambda = 1.8$ and 2.0 in normalized moment shown in the first plot of the fig. 7. On the contrary, the normalized moment for $\lambda = 2$ and 2.75 varies considerably, but C_p differs by a small margin. These differences are be attributed mainly to the changes in rotational speed and subsequently to the operating point.

3.2 Urban terrain simulations under turbulent inflow

This section analyzes the flow field in the urban terrain under application of a log law wind profile and inflow turbulence, and without wind turbines. ~~However, the~~ results from these studies are the basis for the wind turbine investigations in turbulent urban conditions in the following subsection.

The averaged flow variables are analyzed in two different planes along the flow direction at the rooftops of the building A and B. The plane Y=0 m passes through approximately the middle of the A while plane Y=110 m passes through the left part of the B relative to the flow direction. The flow field is averaged for approx. four minutes after the turbulence is propagated through the domain and is fully developed. Fig. 9 shows the distribution of the averaged flow field at building A and building B. Based on the accelerated velocity region, the location for the wind turbines are selected as X= -27 m and X= 0 m at the
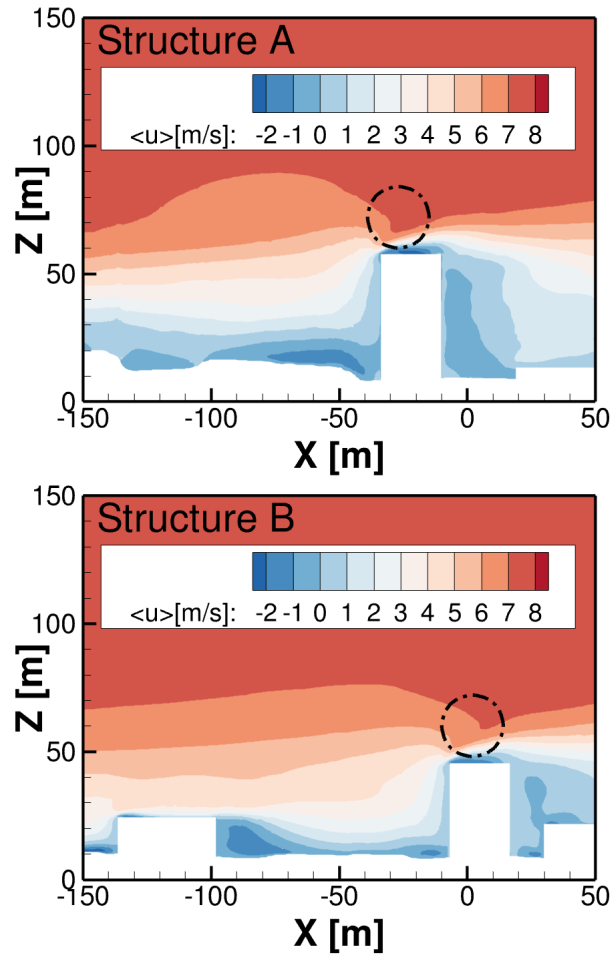
Figure 9. Distribution of averaged u component of velocity in the Plane Y = 0 m and Y = 110 m passing through building A and B

rooftop of A and B, respectively. For the wind turbine investigations later, 10 m, 12 m, and 20 m heights from the rooftop to the center of the blade heights are chosen as discussed in section 2.5.

The velocity profiles and standard deviations at the selected positions over the rooftop of A and B are shown in fig. 10. At the 10 m and 12 m heights, the standard deviations are higher than the 20 m position, which is evident as these positions are

290 close to the rooftop. Along with the upstream turbulence originating from vegetation and topography, the separation caused due to the leading edges influences the nearby rooftop region. The averaged wind speeds and turbulence intensities at different heights from the rooftop are shown in table 2. With increasing distance from the rooftop, the magnitude of mean wind speed increases slightly while the drop in turbulence intensity is observed. Fig. 11 shows the skew angles at different heights above the rooftops of A and B. The near rooftop positions are expected to experience higher skew angles than away positions. The
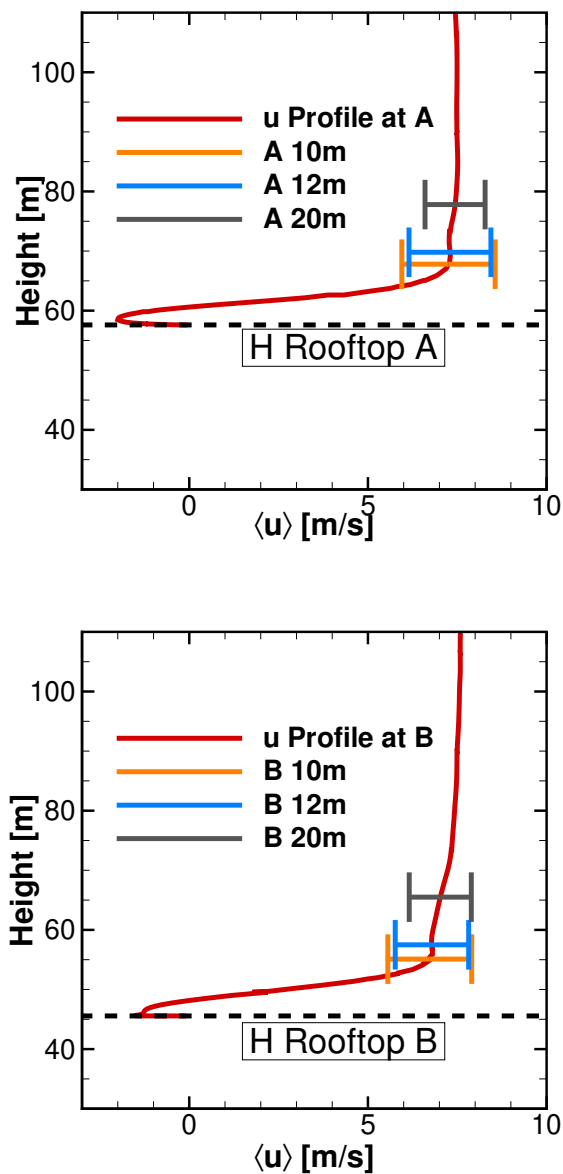
Figure 10. Mean velocity Profile and standard deviations at positions above rooftops of A and B

maximum skew angle of approx. 12.5° occurs at the height of 10 m over the rooftop of A. In general, the flow over A's rooftop appears to be more skewed than over the rooftop of B

For the positions above the rooftops of A and B, time series of u component of velocities are shown in fig. 13, for which the wind turbines are simulated. The power spectral density S_{uu} for the u component is shown in fig. 12. The curves at all turbine
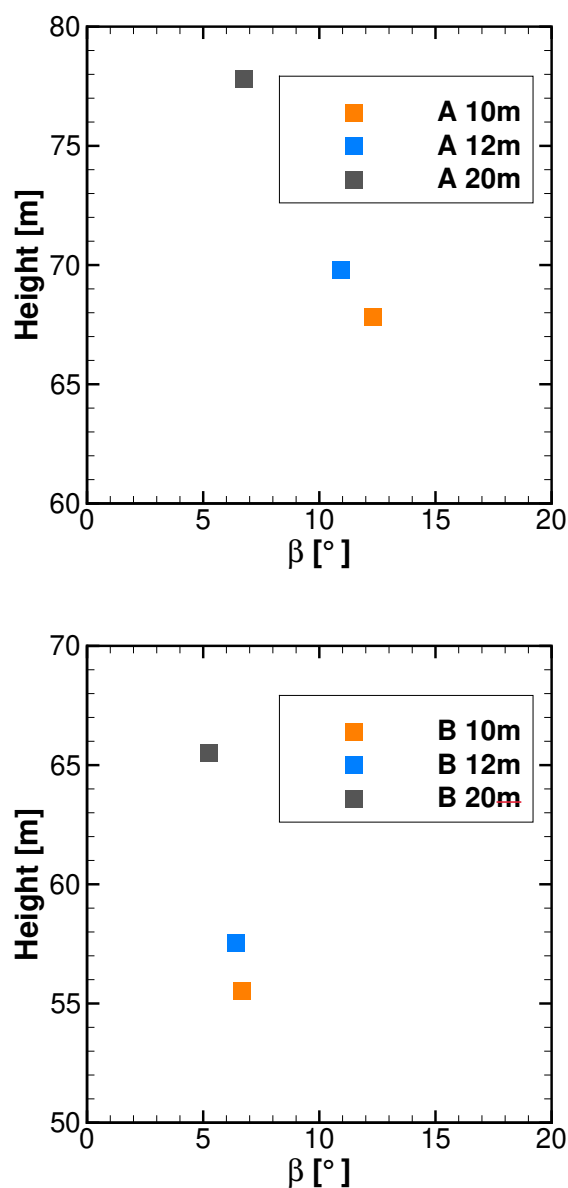
Figure 11. Skew angles at wind turbine positions

positions show good agreement in the region of the inertial range of scales with the Kolmogorov $f^{-5/3}$ spectrum. It indicates

300   that the turbulence is propagated effectively through the domain till the relevant positions of the wind turbines.
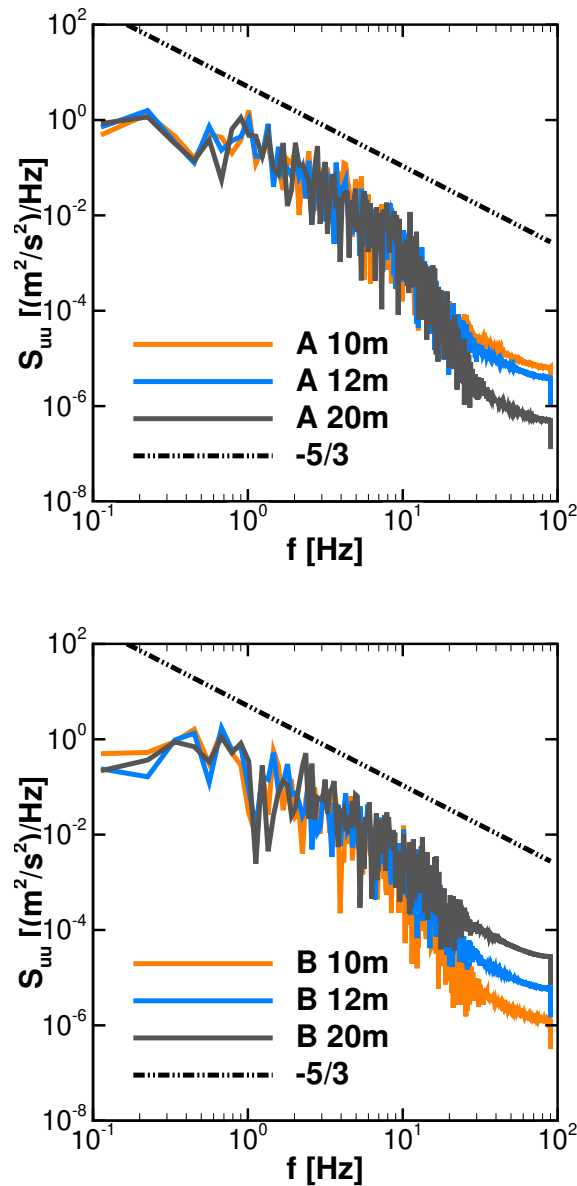
Figure 12. Power spectral density S_{uu} of u component of the velocity at wind turbine positions

3.3 Wind turbines simulations in urban terrain

This section presents the analysis of the wind turbine at different heights above the rooftops of A and B under turbulent inflow.
As discussed in section 2.5, the wind turbines are initialized in the developed turbulent flow field and simulated further. The
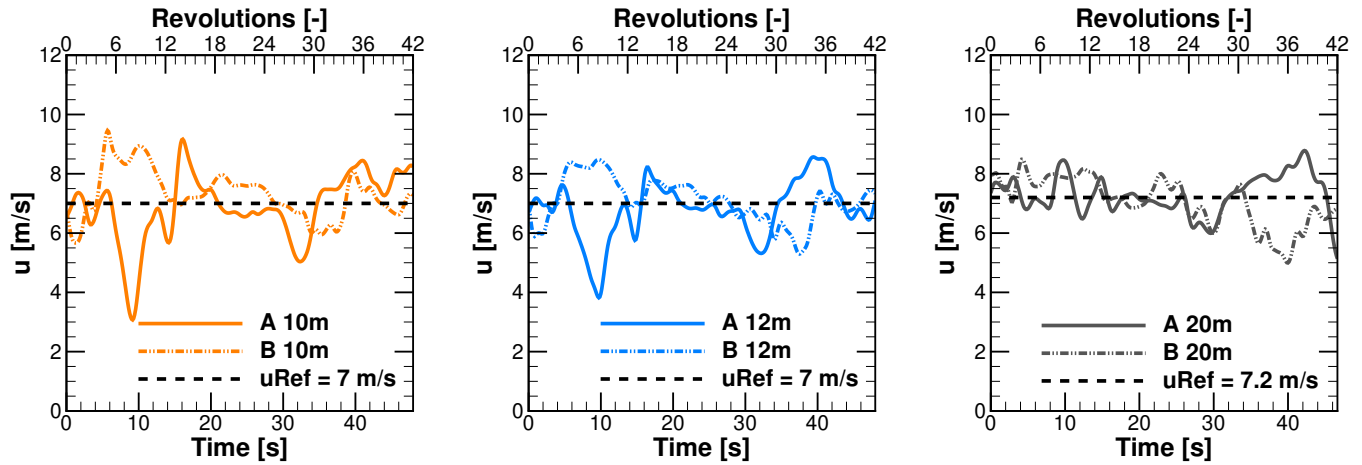
Figure 13. Time series of u component of velocities at different rooftop heights above building A and B

Table 2. Mean wind speeds and turbulence intensities at rooftop

Case name	Mean wind speed (ms^{-1})	Turbulence intensity (%)
A 10 m	7.26	15.24
A 12 m	7.29	13.82
A 20 m	7.45	9.52
B 10 m	6.77	13.94
B 12 m	6.78	12.99
B 20 m	7.02	10.65

objective of these simulations is to investigate the behavior of the H-Darrieus wind turbine under the turbulent inflow influence
305 by the vegetation and the topography of the urban terrain.

At the considered heights, the long averaged wind speeds vary slightly from each other in the range ± 0.5 ms^{-1}, as shown
in the table 2. Also, for the considered time series for the wind turbine investigations, the velocity fluctuates roughly around
the respective mean values except for some large deviations. Therefore, it was assumed that the wind turbines positioned at 10
m, 12 m heights above rooftops of A and B operate at a mean wind speed of 7 ms^{-1} and other positioned at 20 m heights
310 operate at a mean wind speed of 7.2 ms^{-1}. Later, the same values are used for the normalization of the forces and the moments.
Subsequently, the rotational speeds are deduced depending on the wind speed and the operating point of $\lambda = 2.75$. The selected
tip speed ratio $\lambda = 2.75$ lies near to the optimum λ. The variables are averaged after 12 revolutions so that the near wake flow
field of the wind turbine is well developed. The variables are recorded for total of 42 revolutions. However, last 30 revolutions
are considered for the analysis.
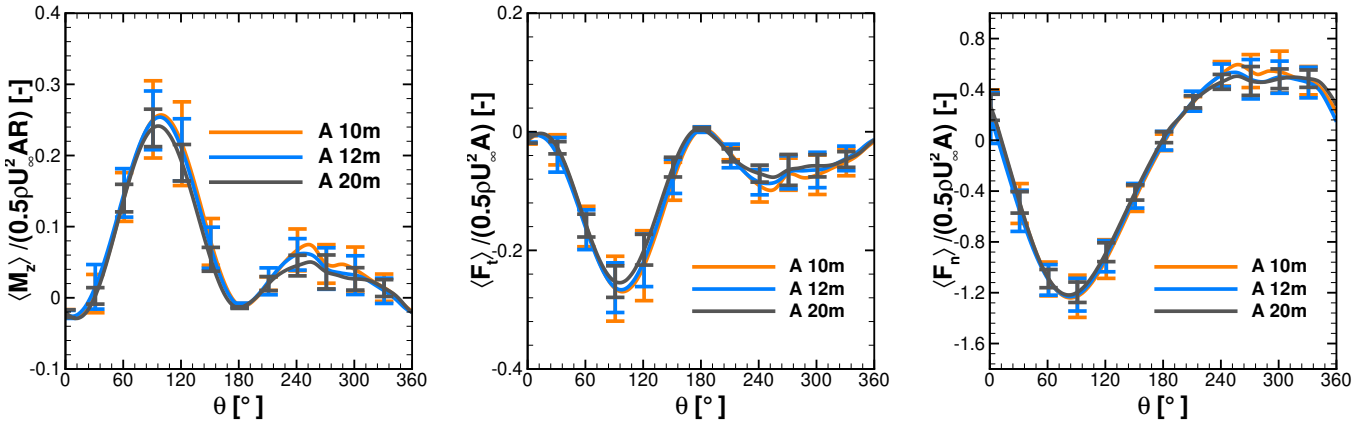
Figure 14. Normalised moment, tangential and normal forces of a single blade at $\lambda = 2.75$ under turbulent inflow at rooftop of A
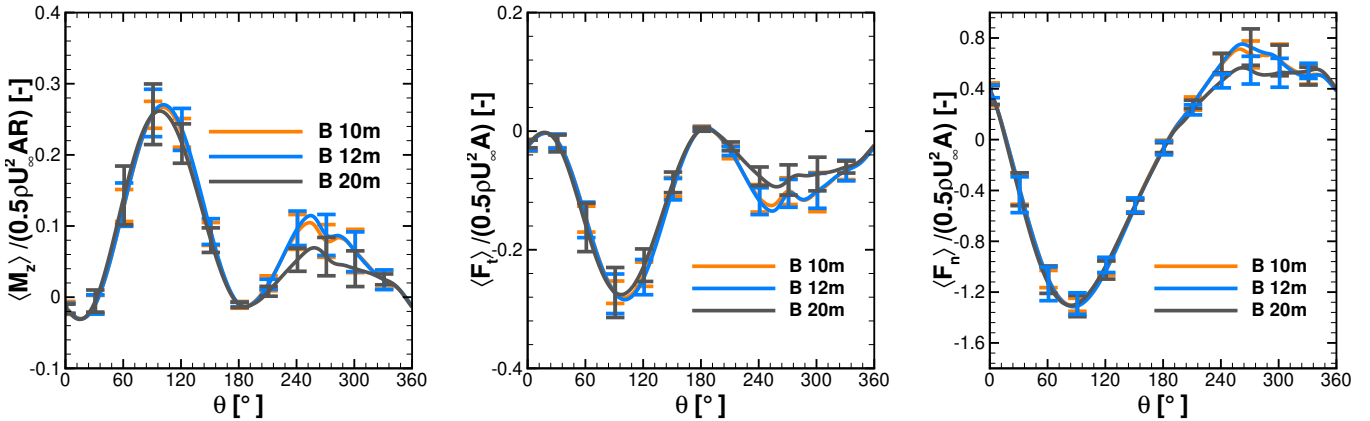
Figure 15. Normalised moment, tangential and normal forces of a single blade at $\lambda = 2.75$ under turbulent inflow at rooftop of B

315   The fig. 14 and fig. 15 show the averaged normalized moment, tangential, and normal forces of a single blade and the standard deviation for the wind turbine at different heights over the rooftop of A and B. The first plot in fig. 14 represents the averaged normalized moment at 10 m, 12 m, and 20 m height above the rooftop of building A. At all three positions, the averaged moments show identical characteristics for the first half revolution. However, the standard deviation contours reveal that the moment deviates significantly around azimuth position 60-120° and 240-300°. Compared with the normalized moment

320 from fig. 7 with the uniform inflow case of $\lambda = 2.75$, the normalized moment of H-VAWT for all heights above the rooftop of A exhibit non-flat characteristic in the second half revolutions implying the improvement in the performance, particularly around azimuth $200° \leq \theta° \leq 270°$. Figure 15 also reveals a consistent trend for a normalized moment over the second half revolution
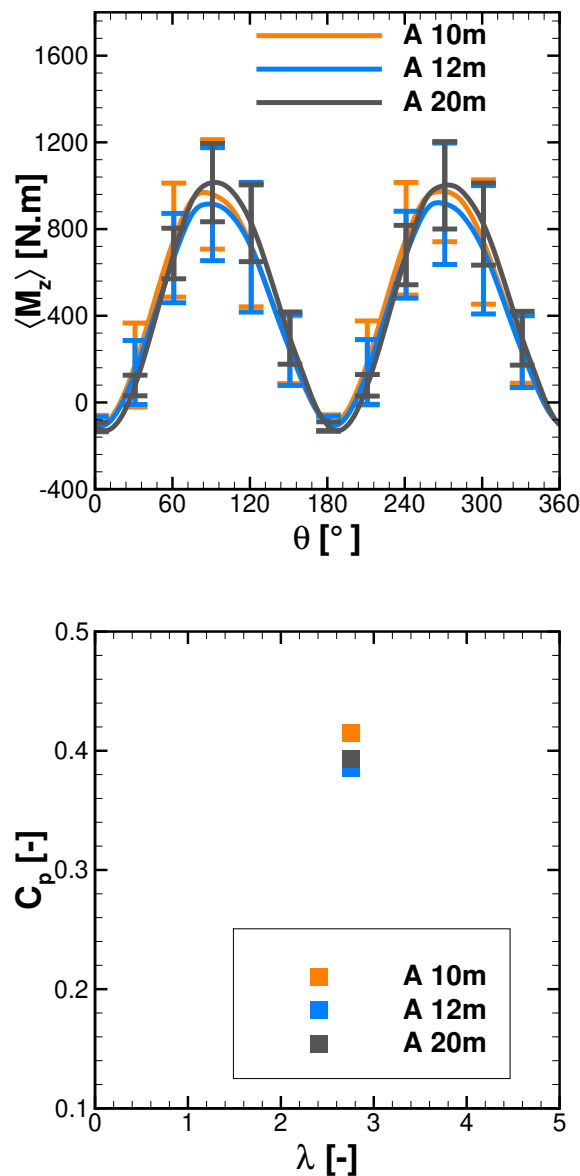
Figure 16. Moment of the complete Rotor and power coefficient at different heights over rooftop of A

The wind turbine moments at the heights 10 m and 12 m above the rooftop of B show significant improvements in the latter half revolution. It is attributed to the skewed flow near to the rooftop heights. Due to the skew angle for flow, the bottom part of
325   the blade in the downwind section is less impacted by the upwind passage of the other blade. Therefore, the reduced blade wake interaction in downwind section improves the performance by generating positive moment. It is also in line with the findings
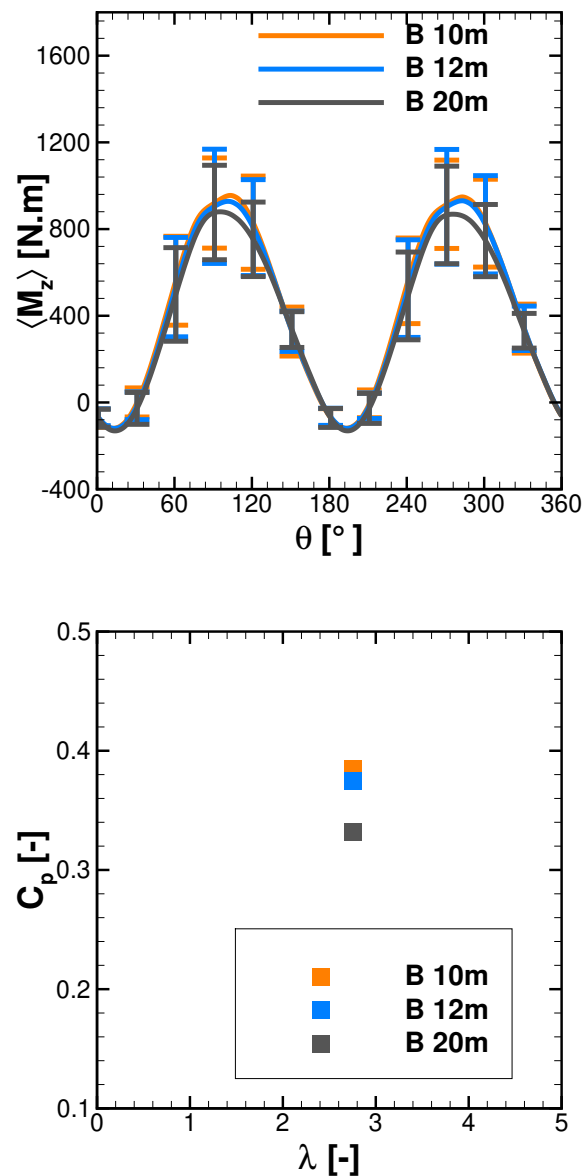
Figure 17. Moment of the complete Rotor and power coefficient at different heights over rooftop of B

of Mertens et al. (2003) that the performance coefficient of an H-Darrieus wind turbine in skewed flow, based on the projected frontal rotor area, can increase above that for non-skewed flow. Orlandi et al. (2015) investigated H-rotor with 3D URANS approach in skewed flow and reported a similar phenomenon in moment and forces. The second plots from fig. 14 and fig. 15

330 present the normalized tangential forces experienced by a single blade at A and B. Showing correlation to the moment, the high

standard deviations are seen in the first half revolutions, including at peak position around 90-95° implying the influence by the complex inflow conditions. Also, in the second half revolutions, the tangential forces show higher magnitudes and standard deviations than the uniform inflow case of $\lambda = 2.75$. The higher magnitude of the standard deviation indicates that blade wake interaction is not periodic in nature like the uniform inflow case. Despite experiencing complex operating conditions near

335 rooftop heights, the averaged moments and tangential forces of a single blade do not show significant difference. The third plots from fig. 14 and fig. 15 show the normalized normal forces experienced by a single blade at different heights above the rooftop of A and B. The lower magnitudes of standard deviations and overlapping curves for the different heights for the first half revolutions indicate that normal forces are less sensitive to turbulence and skewed inflow. However, in the second half revolutions, the increase in the normal forces around azimuth 240-270° for heights above B building can be seen. Due to the

340 skew angles, the blade experiences relatively higher velocities in downwind passage than in uniform inflow case, and at these azimuth positions, the blade chord is almost perpendicular to the flow direction. It results in a small increase in the normal forces.

Figure 16 and fig. 17 present the averaged moment over 30 revolutions for the complete rotor and power coefficient based on it, at different heights over the rooftop of A and B. The moment plots of the complete rotor and standard deviation indicate

345 that the complex inflow conditions significantly impact wind turbine performance. For the peak position around 90-95° and 270-275°, it can be observed that the upper and lower limits lie in the range of approx. $\pm 20 - 25\%$. At the azimuth positions 0° $\pm 30°$ and 180° $\pm 30°$, the standard deviation is small. It can be explained by the lower angle of attack arising from the blade's position parallel to the flow direction. The wind turbines generate more moments at the rooftop of A than B for the shown time series in fig. 13. The coefficients of power are shown in the second plot of fig. 16 and 17. As the power extracted

350 by the wind turbine is directly proportional to the power of wind speed, the overall sum of a positive deviation and negative deviation in the wind speed leads to a positive increase in power. It can be illustrated by a simple mathematical expression as $(a+b)^3 - a^3 > a^3 - (a-b)^3$. It translates that even if the mean wind speed is the same, the higher turbulence case will contain more power (Möllerström et al., 2016). Figure 16 and 17 show that wind turbines perform better at near rooftop heights above buildings A and B. For a fixed λ for an H-VAWT, over a reasonable range of free-stream velocities, the coefficient of

355 power increase with the increase in free-stream velocity. In the present work, even though the averaged wind speeds at all considered heights are lower than the uniform inflow case, the coefficients of power are still higher than that of the uniform case of $\lambda = 2.75$ shown in fig. 8. It is attributed to the combined impact of the turbulence and the skewed flow. At near rooftop heights above building A and B, the H-VAWT shows a significant increase in performance. Figure 18 shows the resolved wake of H-VAWT in turbulent inflow at a height of 10m above building B.

360 **4 Conclusions**

In the present paper, a numerical investigation of the influence of the complex and urban terrain on the behavior of the rooftop mounted VAWT under turbulent inflow conditions are performed. With the help of high-fidelity scale resolving DDES simulation and higher order numerical scheme, the in-stationary characteristics of the forces and moment are studied. The
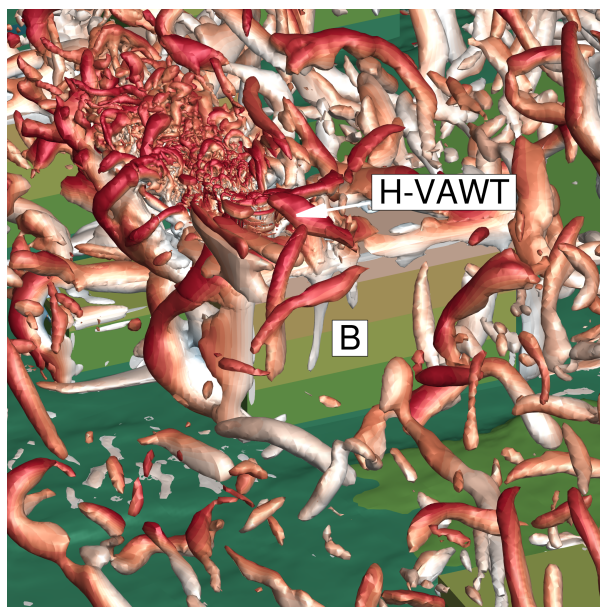
Figure 18. Wake of H-VAWT in turbulent inflow (at $\lambda_2 \pm 0.025$)

behavior of the scaled-up, generic, two straight ~~balded~~ H-VAWT with NACA0021 airfoil is investigated at different locations,

365 with a diameter of 7 m, blade length of 4.2 m, and a fixed pitch angle of 6°. In the first study, the H-VAWT is analyzed under uniform flow conditions of 8 ms^{-1} without inflow turbulence in order to get the operating range of tip speed ratio. It is one the basis for the selection of operating λ for the subsequent studies in the urban terrain.

The second study investigates the flow field in the realistic terrain consisting of different buildings, vegetation, and topographical features under turbulent inflow. Based on the mean wind profiles and turbulence levels, possible locations above

370 the rooftops of two distinct buildings are considered for H-VAWT investigations. In the latter study, the wind turbines are placed in the turbulent flow field at different heights above the rooftop of buildings by applying overlapping grid technique and simulated further. By this simulation strategy, the wind turbines can be investigated in a turbulent flow field with convenience and a significant reduction in the computation cost. In a subsequent study, the characteristics of the H-VAWT is studied for the tip speed ratio $\lambda = 2.75$ in urban terrain.

375 Based on the averaged forces and moments over multiples revolutions, the H-VAWT shows significant improvement in the performance at heights of 10 m and 12 m from the rooftop of buildings. At these heights, it operates in the flow with a relatively higher level of turbulence and skewed angle than the 20 m height. Due to the skewed flow, the reduced blade wake interaction in the second half revolutions (downwind) increases tangential forces and moment extraction compared to the uniform non-skewed flow case. Large deviations are observed in the tangential forces and moments due to temporal changes.

380 The improvement in the performance at near rooftop heights is attributed to the combined influence of the turbulence and skewed angle of the flow. Also, the H-VAWT placed at the height of 20 m from rooftops shows a better power coefficient than

the uniform inflow conditions. Therefore, it can be concluded that turbulence has a positive impact on performance. For the given dimensions of H-VAWT, urban terrain, time series, tip speed ratio λ, and the considered heights for the analysis, the performance increases.

385 *Data availability.* The data about original generic H-VAWT are available from Li et al. (2016). The wind atlas Data used to define log law profile is obtained from the "New European Wind Atlas, a free, web-based application developed, owned and operated by the NEWA Consortium. For additional information see www.neweuropeanwindatlas.eu.

Author contributions. PZ conducted the CFD investigations and wrote the paper. TL initiated the research, supervised the work and revised the manuscript.

390 *Competing interests.* The authors declare that they have no conflict of interest.

Acknowledgements. The authors gratefully acknowledge the High Performance Computing Center Stuttgart for providing computational resources within the project WEALoads. The studies where conducted for the project "Loads and performance of the small wind turbine in urban environment" under "WindyCities" joint graduate research training program funded by Ministry of Science, research and arts, Baden Württemberg. Also, the authors acknowledge Amgad Dessoky for providing the original computation grids of the wind turbine from the
395 validation study.

References

Balduzzi, F., Bianchini, A., Carnevale,E.A, Ferrari L., and Magnani, S.: Feasibility analysis of a Darrieus vertical-axis wind turbine installation in the rooftop of a building, Applied Energy, 97, 921-929, https://doi.org/10.1016/j.apenergy.2011.12.008., 2011

Mithraratne, N.: Roof-top wind turbines for microgeneration in urban houses in New Zealand, Energy and Buildings, 41, Issue 10, 1013-1018, https://doi.org/10.1016/j.enbuild.2009.05.003., 2009

van Wijk, B. M.:Predicting the rooftop wind climate for urban wind energy in the Rotterdam - Delft - Zoetermeer region: new approaches for implementing urban height data in the wind atlas method, Master Thesis, TU Eindhoven/TU Delft,Netherlands, 136 pp., 2011

Toja-Silva, F., Colmenar-Santos, A., and Castro-Gil, M.: Urban wind energy exploitation systems: Behaviour under multidirectional flow conditions—Opportunities and challenges, Renewable and Sustainable Energy Reviews, 24, 364-378, https://doi.org/10.1016/j.rser.2013.03.052. 2013

KC, A., Whale, J., and Urmee, T.: Urban wind conditions and small wind turbines in the built environment: A review, Renewable Energy, 131, 268-283, 0960-1481, https://doi.org/10.1016/j.renene.2018.07.050., 2019

Karadag, I., and Yuksek, I. : Wind Turbine Integration to Tall Buildings, Renewable Energy - Resources, Challenges and Applications, IntechOpen, DOI: 10.5772/intechopen.91650, 2020

Bianchi, S., Bianchini, A., Ferrara, G., and Ferrari, L. : Small Wind Turbines in the Built Environment: Influence of Flow Inclination on the Potential Energy Yield. Proceedings of the ASME Turbo Expo 2013: Turbine Technical Conference and Exposition. Volume 8, https://doi.org/10.1115/GT2013-95637, 2013

Mertens, S., van Kuik, G., and van Bussel, G.: Performance of an H-Darrieus in the Skewed Flow on a Roof." ASME. J. Sol. Energy Eng. November 2003; 125(4): 433–440. https://doi.org/10.1115/1.1629309

Möllerström, E., Ottermo, F., Goude, A., Eriksson, S., Hylander, J., and Bernhoff H.:Turbulence influence on wind energy extraction for a medium size vertical axis wind turbine, Wind Energ. 2016; 19:1963–1973, DOI: 10.1002/we.1962, 2016

Bertényi, T., Wickins, C., and McIntosh, S.: Enhanced Energy Capture Through Gust-Tracking in the Urban Wind Environment, 48th AIAA Aerospace Sciences Meeting Including the New Horizons Forum and Aerospace Exposition, Doi:10.2514/6.2010-1376, 2016

Pagnini, L.c., Burlando, M.,and Repetto, M.P. : Experimental power curve of small-size wind turbines in turbulent urban environment, Applied Energy, Volume 154, 112-121, Doi: https://doi.org/10.1016/j.apenergy.2015.04.117., 2015

Kooiman, S., and Tullis, S.: Response of a Vertical Axis Wind Turbine to Time Varying Wind Conditions Found within the Urban Environment. Wind Engineering. 34. 10.1260/0309-524X.34.4.389, 2010

Trivellato, F., and Castelli, M. R.: On the Courant–Friedrichs–Lewy criterion of rotating grids in 2D vertical-axis wind turbine analysis, Renewable Energy, 62, 53-62, Doi https://doi.org/10.1016/j.renene.2013.06.022., 2014

Balduzzi, F., Bianchini, A., Ferrara, G., and Ferrari, L.: Dimensionless numbers for the assessment of mesh and timestep requirements in CFD simulations of Darrieus wind turbines, Energy, 97, 246-261, https://doi.org/10.1016/j.energy.2015.12.111., 2016

Balduzzi, F., Drofelnik, J., Bianchini, A., Ferrara, G., Ferrari, L., and Campobasso, M. S.: Darrieus wind turbine blade unsteady aerodynamics: a three-dimensional Navier-Stokes CFD assessment, Energy, Volume 128, 550-563, https://doi.org/10.1016/j.energy.2017.04.017. , 2017

Lam, H.F., and Peng, H.Y. : Study of wake characteristics of a vertical axis wind turbine by two- and three-dimensional computational fluid dynamics simulations, Renewable Energy, Volume 90, Pages 386-398, https://doi.org/10.1016/j.renene.2016.01.011., 2016

Dessoky, A., Bangga, G., Lutz, T., and Krämer, E., Computational Study Using DDES with Higher Order Scheme Modeling to Predict Darrieus VAWT Noise Mechanisms. In New Results in Numerical and Experimental Fluid Mechanics XII; Springer Science and Business Media LLC: Berlin/Heidelberg, Germany, 2019; Volume 142, pp. 807–818.

435   Patil, R.; Daróczy, L.; Janiga, G.; Thévenin, D.: Large eddy simulation of an H-Darrieus rotor. Energy 2018, 160, 388–398.

Brahimi, M. T., and Paraschivoiu, I. (May 1, 1995). "Darrieus Rotor Aerodynamics in Turbulent Wind." ASME. J. Sol. Energy Eng. May 1995; 117(2): 128–136. https://doi.org/10.1115/1.2870839

M. Salman Siddiqui, Adil Rasheed, Trond Kvamsdal, Mandar Tabib, Effect of Turbulence Intensity on the Performance of an Offshore Vertical Axis Wind Turbine, Energy Procedia, Volume 80, 2015, Pages 312-320, ISSN 1876-6102,

440   https://doi.org/10.1016/j.egypro.2015.11.435.

Abdolrahim Rezaeiha, Hamid Montazeri, Bert Blocken, Characterization of aerodynamic performance of vertical axis wind turbines: Impact of operational parameters, Energy Conversion and Management, Volume 169, 2018, Pages 45-77, ISSN 0196-8904, https://doi.org/10.1016/j.enconman.2018.05.042.

M. Salman Siddiqui, Muhammad Hamza Khalid, Rizwan Zahoor, Fahad Sarfraz Butt, Muhammed Saeed, Abdul Waheed Badar, A numerical

445   investigation to analyze effect of turbulence and ground clearance on the performance of a roof top vertical–axis wind turbine, Renewable Energy, Volume 164, 2021, Pages 978-989, ISSN 0960-1481, https://doi.org/10.1016/j.renene.2020.10.022.

A. Orlandi, M. Collu, S. Zanforlin, A. Shires, 3D URANS analysis of a vertical axis wind turbine in skewed flows, Journal of Wind Engineering and Industrial Aerodynamics, Volume 147, 2015, Pages 77-84, https://doi.org/10.1016/j.jweia.2015.09.010.

Q. Li, T. Maeda, Y. Kamada, J. Murata, M. Yamamoto, T. Ogasawara, K. Shimizu, T. Kogaki, Study on power performance for

450   straight-bladed vertical axis wind turbine by field and wind tunnel test, Renewable Energy, Volume 90, 2016, Pages 291-300, https://doi.org/10.1016/j.renene.2016.01.002.

P. Letzgus, T. Lutz, E. Krämer Detached Eddy Simulations of the local Atmospheric Flow Field within a Forested Wind Energy Test Site located in Complex Terrain, Journal of Physics: Conference Series, Volume 1037, 2018, Pages 072043, https://doi.org/10.1088/1742-6596/1037/7/072043.

455   R.H.Shaw, U. Schumann Large-eddy simulation of turbulent flow above and within a forest, Boundary-Layer Meteorology, Volume 61, 1992, Pages 47-64, https://doi.org/10.1007/BF02033994.

J. Mann Wind field simulation, Probabilistic Engineering Mechanics, Volume 13, 1998, Pages 269-282, https://doi.org/10.1016/S0266-8920(97)00036-2

N. Troldborg, J. N. Sørensen, R. Mikkelsen, N. N. Sørensen A simple atmospheric boundary layer model applied to large eddy simulations

460   of wind turbine wakes, Wind Energy, Volume 17, 2014, Pages 657-669, https://doi.org/10.1002/we.1608

C. Rossow, N. Kroll, D. Schwamborn The MEGAFLOW Project – Numerical Flow Simulation for Aircraft, Progress in Industrial Mathematics at ECMI 2004, 2006, Pages 3-33

J. Benek, P. Buning, J. Steger A 3-D chimera grid embedding technique, 7th Computational Physics Conference, 1985, https://doi.org/10.2514/6.1985-1523

465   U. Schäferlein, C. Oehrle, M. Hollands, M. Keßler, E. Krämer, Computation of Helicopter Phenomena Using a Higher Order Method, 2013, Pages 423-438, https://doi.org/10.1007/978-3-319-02165-2_29

P. Weihing, J. Letzgus, G. Bangga, T. Lutz, E. Krämer, Hybrid RANS/LES Capabilities of the Flow Solver FLOWer—Application to Flow Around Wind Turbines, Progress in Hybrid RANS-LES Modelling, 2018, Pages 369-380, https://doi.org/10.1007/978-3-319-70031-1_31

R. F. Menter, Two-equation eddy-viscosity turbulence models for engineering applications, AIAA Journal, volume = 32, 1994, Pages
470   1598-1605, https://doi.org/10.2514/3.12149

A. Jameson, W. Schmidt, E. Turkel, Numerical solution of the Euler equations by finite volume methods using Runge Kutta time stepping
schemes, 14th Fluid and Plasma Dynamics Conference, 1981, volume = 32, https://arc.aiaa.org/doi/abs/10.2514/6.1981-1259

R. Bravo, S. Tullis, S. Ziada, S., Performance Testing of a Small Vertical-Axis Wind Turbine, Proceedings of the 21st Canadian Congress of
Applied Mechanics (CANCAM07), 2007

475   I. Baring-Gould, J. Fields, F. Oteri, R. Preus, Deployment of Wind Turbines in the Built Environment: Risks, Lessons, and Recommended
Practices, 2017, https://www.osti.gov/biblio/1361457

C. J. Ferreira, H. Bijl, G. van Bussel, G. van Kuik, Simulating Dynamic Stall in a 2D VAWT: Modeling strategy, verification and validation
with Particle Image Velocimetry data, 2007, Volume = 75, Pages 012023, Journal of Physics: Conference Series, https://doi.org/10.1088/
1742-6596/75/1/012023

480   G. Bangga, T. Lutz, A. Dessoky, E. Krämer Unsteady Navier-Stokes studies on loads, wake, and dynamic stall characteristics
of a two-bladed vertical axis wind turbine, 2017, Volume 9, pages 053303, Journal of Renewable and Sustainable Energy,
https://doi.org/10.1063/1.5003772

L. Kern, J.V. Seebaß, J. Schlüter, Das Potenzial von vertikalen Windenergieanlagen im Kontext wachsender Flächennutzungskonflikte
und Akzeptanzprobleme der Windenergie, 2019, Volume 43, pages 289-302, Zeitschrift für Energiewirtschaft,
485   https://doi.org/10.1007/s12398-019-00264-7